Mansoura Engineering Journal

Volume 49 | Issue 1 Article 3

October 2023

Spatio-temporal Analysis Mapping of Air Quality Monitoring in Cairo using Sentinel-5 satellite data and Google earth engine

Sara Sameh
Faculty of Engineering and Technology, Badr University in Cairo (BUC), Cairo, Egypt,
sara.sameh@buc.edu.eg

Fawzi Zarzoura
Public Works Engineering Department, Faculty of Engineering, Mansoura University, Mansoura 35516, Egypt

Mahmoud El-Mewafi
Public Works Engineering Department, Faculty of Engineering, Mansoura University, Mansoura 35516, Egypt

Follow this and additional works at: https://mej.researchcommons.org/home

 Part of the Architecture Commons, and the Engineering Commons

Recommended Citation

Sameh, Sara; Zarzoura, Fawzi; and El-Mewafi, Mahmoud (2023) "Spatio-temporal Analysis Mapping of Air Quality Monitoring in Cairo using Sentinel-5 satellite data and Google earth engine," *Mansoura Engineering Journal*: Vol. 49 : Iss. 1 , Article 3.
Available at: https://doi.org/10.58491/2735-4202.3122

This Review is brought to you for free and open access by Mansoura Engineering Journal. It has been accepted for inclusion in Mansoura Engineering Journal by an authorized editor of Mansoura Engineering Journal. For more information, please contact mej@mans.edu.eg.

REVIEW

Spatio-temporal Analysis Mapping of Air Quality Monitoring in Cairo Using Sentinel-5 Satellite Data and Google Earth Engine

Sara Sameh [a,b,*], Fawzi Zarzoura [b], Mahmoud El-Mewafi [b]

[a] Faculty of Engineering and Technology, Badr University in Cairo (BUC), Cairo, Egypt
[b] Public Works Engineering Department, Faculty of Engineering, Mansoura University, Mansoura, Egypt

Abstract

Air pollutants including nitrogen dioxide (NO_2), carbon monoxide (CO), and sulphur dioxide (SO_2) cause serious damage to human health and the environment. This research aims to assess built-up seasonal variations of air pollution maps over Cairo city in Egypt using remote sensing data. Land Surface Temperature (LST) data was obtained from the MODIS Terra Satellite data, specifically the MOD11A1 V6 product, from January to December 2022. The Sentinel-5 project utilizes the tropospheric monitoring instrument (TROPOMI) sensor to capture images across different spectral bands, enabling precise monitoring of air pollution levels. The concentration data of NO_2, CO, and SO_2 were extracted from Sentinel-5P using Google Earth Engine (GEE), which was utilized extensively in this study. The study found that the eastern region had the highest levels of NO_2 and CO emissions, attributed to transportation and heating in densely populated areas. The northern region had the highest SO_2 emissions due to industrial activities. Higher pollution levels were observed during colder months, which can be attributed to the temperature version phenomenon. However, summer pollutants pose greater health risks to humans. The statistical analysis showed a positive correlation between average pollutant concentrations (NO_2, CO, SO_2) and mean LST in 2022, with R-squared values indicating moderate associations (0.3757 for NO_2, 0.2865 for CO, and 0.1774 for SO_2). Additionally, the exponential smoothing (ETS) algorithm was employed to forecast a time series, and the results were evaluated by comparing the original and predicted values, calculating the root-mean-square (RMS) error to validate the approach. The findings demonstrate that the ETS is highly effective and precise. Our study provides a spatio-temporal analysis of air quality monitoring in Cairo using Sentinel-5 satellite data and highlights the spatial and temporal patterns of NO_2 concentrations and LST in the region. The findings of the study indicate that Cairo City's air quality is significantly compromised because of urban expansion, the rise in vehicular activity, and the rapid growth of industries. Consequently, the deteriorating air quality directly contributes to the city's climate change issues.

Keywords: Air quality, Google earth engine (GEE), Land surface temperature (LST), Sentinel 5p, Tropospheric monitoring instrument (TROPOMI)

1. Introduction

Climate change has become increasingly concerning due to the impact of air pollution on the global environment, with anthropogenic sources releasing greenhouse gases like carbon dioxide and methane contributing to its acceleration (IPCC, 2021). The primary causes of air pollution are urbanization, energy consumption, transportation, and motorization, which negatively impact the environment and human health (Liu et al., 2022). According to the most common air pollutants are Carbon Monoxide (CO), particulate matter (PM), sulfur dioxide (SO_2), nitrogen dioxide (NO_2), ozone (O_3), and carbon dioxide (Nouri et al., 2023). High concentrations of these pollutants can cause serious health problems such as pulmonary and cardiovascular diseases (Wen et al., 2023). The combustion

Received 23 July 2023; revised 16 September 2023; accepted 27 September 2023.
Available online 2 November 2023

* Corresponding author.
E-mail address: sara.sameh@buc.edu.eg (S. Sameh).

https://doi.org/10.58491/2735-4202.3122
2735-4202/© 2024 Faculty of Engineering, Mansoura University. This is an open access article under the CC BY 4.0 license (https://creativecommons.org/licenses/by/4.0/).

of gasoline and diesel fuels in vehicles gives rise to a varied mixture of gaseous and particulate pollutants, which have adverse effects on human health. These detrimental emissions are intensified during periods of heightened commuting, such as during acceleration, deceleration, and the initial phase of a journey (typically the first 2–3 km). The referred period is when the car engine is still cold, resulting in increased diffusion of CO. Additionally, the emission rate of pollutants can be influenced by meteorological conditions (Kurata et al., 2020).

Air pollution is a major environmental issue in many urban areas around the world, and Cairo is no exception. The city is known for its high levels of air pollution, which are caused by a variety of factors including industrial emissions, vehicular traffic, and natural sources such as dust storms (Mostafa et al., 2021). The health impacts of air pollution in Cairo are significant, with studies showing that exposure to high levels of air pollution can lead to respiratory and cardiovascular diseases, as well as other health problems (Liu et al., 2020).

In recent years, there has been growing interest in the use of remote sensing data for air quality monitoring. Remote sensing techniques allow for the collection of data on air pollution over large areas, which can provide a more comprehensive understanding of air quality than traditional monitoring methods (Hwang et al., 2023). In particular, satellite-based remote sensing has emerged as a powerful tool for air quality monitoring, as it allows for the collection of data on air pollution over large areas regularly (Krotkov et al., 2016). This approach has been used in several studies to monitor air pollution in urban areas around the world, including Cairo (Hereher et al., 2022). However, there is still a need for more research on the use of remote sensing data for air quality monitoring in Cairo, particularly about the spatial and temporal patterns of air pollution in the city.

The tropospheric monitoring instrument (Sentinel-5P TROPOMI) is utilized for technical purposes to estimate anthropogenic emissions and design air pollution abatement strategies. Atmospheric compounds such as NO_2, SO_2, CO, and CH_2O, which are historically and currently being released in large amounts in industrial and urban areas, are of particular interest (Nyaga, 2021). The main source of these emissions is the use of fossil fuels, which has increased the levels of these compounds globally. Among them, NO_2 and CO are known human carcinogens and pose a direct threat to human health (Manisalidis et al., 2020). As the population living in cities continues to grow, the level of pollutants emitted into the atmosphere also increases, leading to adverse health effects that will worsen over time (Nyaga, 2021).

Regarding the choice of air pollutants, we focused on NO_2, SO_2, and CO as these three pollutants have the highest concentrations in Cairo and are major contributors to poor air quality and negative health impacts. Cairo, the capital of Egypt, has a high concentration of these pollutants due to urbanization, energy consumption, transportation, and motorization. NO_2 and SO_2 are known to cause respiratory problems, while CO is a common air pollutant and can be used as an indicator of traffic-related pollution. By focusing on these three pollutants, we aimed to provide a comprehensive understanding of air quality in Cairo and identify areas of high pollution levels to inform policy decisions aimed at reducing air pollution in the city.

CO is generated because of incomplete combustion in various sources, including vehicle operations, heating systems, coal power generation, and the burning of biomass (Hwang et al., 2023). Around 40 % of CO emissions originate from natural sources, including volcanic eruptions, emissions from natural gas, degradation of vegetation and animals, and forest fires (Varma et al., 2009). The remaining 60 % of CO emissions are attributed to various human activities, including fossil fuel consumption, waste disposal, tobacco smoke, and the burning of charcoal fires (Vreman et al., 2000). While outdoor tropospheric CO is generally regarded as not posing a significant health risk, recent studies have indicated a potential link between urban CO exposure and the occurrence of cardiac problems. Satellite-based monitoring of tropospheric CO has been in operation since 1995, utilizing instruments such as the Global Ozone Monitoring Experiment (GOME) designed specifically to observe a variety of gases present in the Earth's stratosphere and troposphere (Burrows et al., 1999). The TROPOMI instrument on the Sentinel 5 Precursor (S5P) satellite monitors the global levels of CO by utilizing measurements of Earth radiance in both clear-sky and cloudy-sky conditions. These measurements are taken in the 2.3 μm spectral range of the shortwave infrared (SWIR) portion of the solar spectrum (Veefkind et al., 2012).

Oxides of nitrogen, including NO_2 and NO, are significant trace gases produced by both human activities and natural processes. These emission gases have harmful effects on the atmosphere, contributing to issues like smog and acid rain. NO_2 and NO exist in the Earth's atmosphere and are introduced into it through both human-related activities and natural events. The TROPOMI NO_2 processing system utilizes advanced algorithms and satellite data to estimate the vertical column of NO_2,

providing valuable insights into atmospheric pollution. It employs a retrieval-assimilation-modeling approach based on the TM5-MP chemistry transport model. The system has been specifically adapted for TROPOMI, utilizing Sentinel-5P satellite data at a high-resolution scale (Baldasano, 2020).

SO_2 is emitted into the atmosphere because of both natural occurrences and human activities. It has significant implications for local and global chemistry and can cause short-term pollution as well as climate-related effects. The increased concentrations of SO_2 in the atmosphere predominantly stem from anthropogenic sources, including vehicle exhaust emissions, the burning of biomass, and the combustion of fossil fuels. These human-related activities contribute to the heightened levels of SO_2 in the atmosphere, alongside natural phenomena such as lightning, forest fires, microbial activities, and other natural processes. Approximately 30 % of SO_2 emissions come from natural sources, with the majority being anthropogenic. These emissions have detrimental impacts on human health and air quality. Furthermore, the presence of SO_2 in the atmosphere affects climate dynamics by contributing to the creation of sulfate aerosols, which in turn exert a significant influence on radiative balance (Krotkov et al., 2016).

Numerous research studies have demonstrated the effectiveness of the TROPOMI instrument since its deployment with the launch of S5P. In a previous investigation, the TROPOMI data was utilized for the monitoring of NO_2 levels over the region of Turkey, and in another study focused on CO measurements, the initial results of using TROPOMI over China were presented, highlighting the capabilities of the instrument (Borsdorff et al., 2018). Statistical analyses comparing TROPOMI data with ground-based measurements on a global scale reveal a minor percentage difference between the two (Garane et al., 2019). In a study conducted in Al-Qurayyat City, Saudi Arabia, it was found that the concentrations of CO and NO_2 measuring from TROPOMI, primarily emitted from vehicular sources, showed a strong correlation, indicating a common emission origin (Al-alola et al., 2022). In a study conducted in Africa, specifically focusing on cities such as Cairo and Algiers, it was found that the TROPOMI satellite instrument, with its daily global coverage and high resolution, successfully identified a weekend effect in road transport-dominated CO emissions (Leguijt et al., 2023). Another study in Greater Cairo, Egypt, using the TROPOMI satellite instrument, found significant correlations between surface urban heat island intensity (SUHII) and NO_2 in spring and CO in winter, highlighting the importance of geospatial technology for analyzing regional air pollution and informing urban environmental management (Hereher et al., 2022).

Furthermore, Egypt's dry climate, characterized by limited rainfall and the prevalence of desert areas, gives rise to seasonal weather conditions laden with sand particles. The combination of these factors, along with pre-existing air pollution, has led to the persistent occurrence of the 'Black Cloud' phenomenon. The 'Black Cloud' phenomenon, is a recurrent issue affecting air quality in Cairo. The 'Black Cloud' refers to a visible haze or smog layer that often envelops the city, primarily during certain seasons. It results from a combination of factors, including high levels of air pollution, adverse weather conditions, and geographical features that trap pollutants within the urban area. This phenomenon has significant implications for public health, the environment, and urban planning, making it a crucial concern for policymakers and researchers alike. The Egyptian Environmental Affairs Agency (EEAA) has made efforts to enhance air quality, with a particular focus on addressing pollution within the cement industry a significant sector in the Egyptian economy. Additionally, the EEAA has implemented measures to manage agricultural waste, specifically targeting the control of large-scale rice straw burning. However, it is important to note that vehicle exhaust emissions represent a substantial source of air pollution, particularly in Cairo where traffic density is high (Abou-Ali and Thomas, 2012).

The novelty of our research lies in the use of Sentinel-5 satellite data to monitor air pollution in Cairo. Unlike previous studies that primarily relied on limited ground-based data, our study introduces a novel approach by utilizing remote sensing data and using the Google Earth Engine (GEE) platform to extract this data. By incorporating remote sensing techniques, we were able to obtain a more comprehensive and extensive understanding of air quality in Egypt. For example, we were able to generate high-resolution maps of air pollution levels across the city, which would not have been possible with traditional monitoring methods. We were also able to analyze the spatio-temporal patterns of air pollution over a longer time period than would have been feasible with ground-based monitoring alone. Additionally, our study provides a spatio-temporal analysis of air pollution in Cairo that can be used to inform policy decisions and interventions aimed at reducing air pollution levels in the city. Overall, our study demonstrates the potential of remote sensing techniques to provide a more detailed and accurate picture of air

quality in urban areas, which can help to improve public health and environmental outcomes.

1.1. Study area

This study aimed to investigate air pollution levels in Cairo, the capital city of Egypt. Cairo, which is the largest metropolis in Egypt, holds the distinction of being the sixth-largest metropolitan area globally and the largest city in Africa, the Middle East, and the Arab world, as demonstrated in Fig. 1. With a population of 21.9 million people, an area spanning 3124.7487 km^2, and a population density of 17 601/km^2, Cairo faces significant challenges due to industrialization and population growth. Consequently, temperatures have seen a notable increase over the past decade. Air pollution in Cairo arises from multiple sources, including the combustion of waste, vehicle emissions (attributable to approximately 4.5 million cars circulating in the city), and urban industrial activities. These factors have contributed to a range of environmental issues associated with aerosol particulate matter, notably with high levels of sulfur dioxide and lead. Consequently, Cairo has been recognized as one of the most polluted cities globally (Rovella et al., 2021).

Specifically, we have highlighted Cairo's status as the capital of Egypt and one of the most populous cities in the world. We have also explained how our survey of the concentration of chosen gases (NO_2, CO, SO_2) all over Egypt found that Cairo has the highest concentration of these pollutants. Furthermore, Cairo is facing significant challenges due to industrialization and population growth, which have contributed to a range of environmental issues associated with aerosol particulate matter, notably with high levels of sulfur dioxide and lead. Consequently, Cairo has been recognized as one of the most polluted cities globally. By studying air pollution in Cairo, we can gain insights into the challenges faced by other urban areas in Egypt and other developing countries.

To address these issues, the EEAA has implemented several management plans to reduce air pollution levels in the city. These include measures to manage agricultural waste, specifically targeting the control of large-scale rice straw burning, and addressing pollution within the cement industry, a significant sector in the Egyptian economy. Additionally, the EEAA has launched awareness campaigns to educate the public on the health impacts of air pollution and encourage them to take action to reduce their exposure. Despite these efforts, air pollution remains a significant challenge in Cairo, and further action is needed to improve air quality in the city.

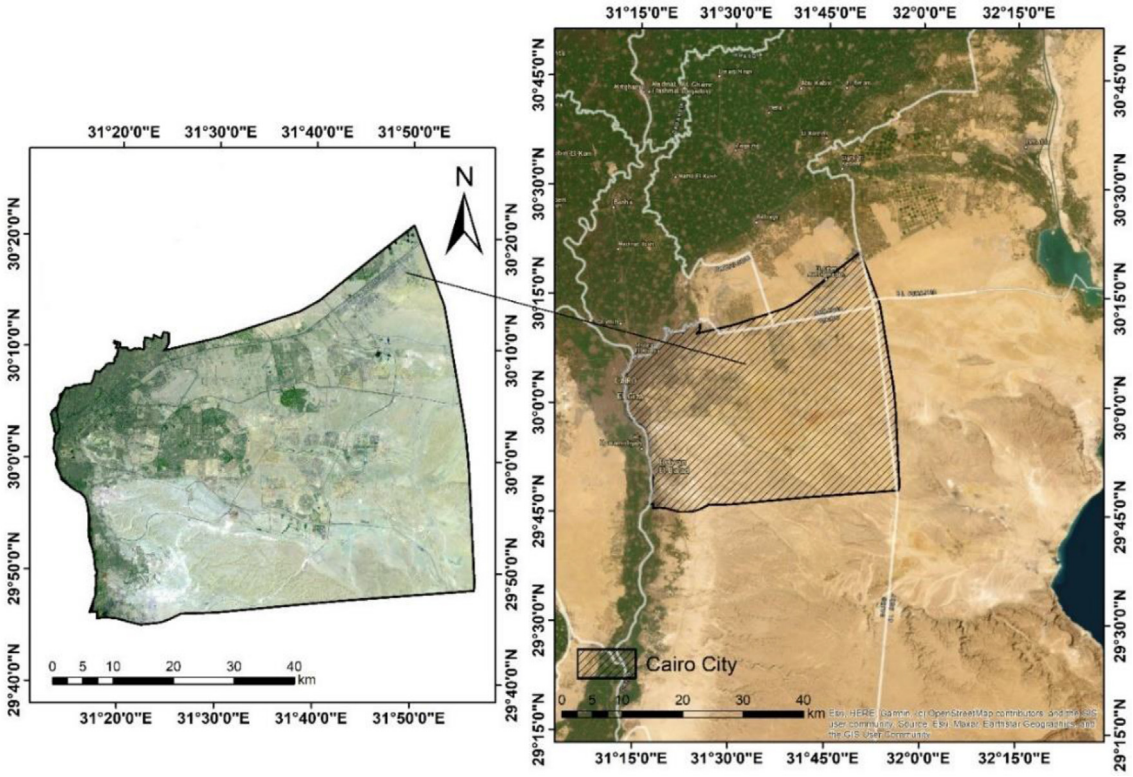

Fig. 1. Study area (Cairo city).

2. Materials and methods

2.1. TROPOMI/sentinel-5p data

The Sentinel-5P satellite incorporates the TROPOMI instrument, a multispectral sensor optimized for tropospheric monitoring. It captures the reflectance of different wavelengths with exceptional precision, enabling the measurement of atmospheric gas concentrations. Operating at a spatial resolution of 0.01 arc degree, TROPOMI provides detailed and accurate data for comprehensive analysis of air quality (Xia et al., 2021). Since its launch on October 13, 2017, as a crucial component of the Copernicus project, TROPOMI has remained operational, continuously gathering valuable information on atmospheric air quality. This instrument is specifically engineered to acquire data essential for both air quality monitoring and climate observations. Throughout its operational period, TROPOMI has diligently recorded daily updates on the state of the atmosphere (Schneising et al., 2023). The data from S5P TROPOMI does not necessitate any further preprocessing before utilization. Equipped with four spectrometers spanning the ultraviolet (UV), visible (UVIS), near-infrared (NIR), and shortwave infrared (SWIR) wavelengths, the instrument enables authorized researchers to access a computerized system and obtain comprehensive insights into the concentration of atmospheric pollutants in specific regions across the world. This access allows for the attribution of detailed information by registered researchers (Bodah et al., 2022). The Sentinel-5P TROPOMI instrument is proficient in monitoring the levels of atmospheric pollutants and trace gases, including NO_2, SO_2, and CO Column Density, that result from human activities and are released into the atmosphere. This advanced technology effectively captures and observes these concentrations, offering valuable insights into the impact of anthropogenic emissions on the atmosphere. Table 1 provides a comprehensive overview of the specifications associated with Sentinel-5P TROPOMI.

2.2. MODIS Terra LST data

MODIS Terra Satellite Data, specifically the MOD11A1.V6 product, was used in this study to estimate the Land Surface Temperature (LST) within the designated study area. Data on Land Surface Temperature (LST) for the period of January to December 2022 were collected from the Land Processes Distributed Active Archive Center, operated by the United States Geological Survey. The archive provided daily composites of LST, which were utilized in this study. Through processing 30 MODIS images per month, individual nighttime layers were compiled, culminating in the creation of monthly average images. To determine the mean value of each pixel within the study area for a given month, all corresponding pixel records were averaged. The GEE Code Editor calibrated image temperatures to degrees Celsius for uniformity. The mean monthly LST photos were clipped to the research area, providing vital insights into how human-generated heat affects LST in the region (Sameh et al., 2023).

2.3. Google earth engine

The present study made use of the GEE and its Code Editor to obtain S5P TROPOMI data and MODIS datasets for computational purposes. GEE, a cloud-based platform designed for large-scale geospatial analysis, facilitated access to a wide range of satellite imagery and geospatial data sources, enabling the monitoring and measurement of environmental changes on a significant scale. By utilizing the computing power of thousands of machines in Google's data centers, GEE provided

Table 1. Specifications of Sentinel-5P tropospheric monitoring instrument.

Band	Spectral Coverage (nm)	Swath width (Km)	Spectral resolution	Temporal resolution	Spatial sampling (km^2)
UV					
1	270–320		0.49	Daily	7 *28
2					
VIS					
3	320–495	2600	0.54		7*3.5
4					
NIR					
5	675–775		0.38		
6					
SWIR					
7	2305–2385		0.25		
8					7*7

parallel-computing capabilities through its Python and JavaScript-based application programming interface (API), empowering scientists to scale up their analyses or develop novel methodologies. Preprocessing techniques were applied to the TROPOMI data, involving cloud cover removal and the application of quality control filters. Following this, the data were transformed into tropospheric vertical column densities and spatially averaged within predefined areas of interest. The extraction and retrieval of pollutant concentration levels from S5P TROPOMI datasets were facilitated by the cloud computing capabilities offered by the GEE platform.

To retrieve the concentration data of NO_2, CO, and SO_2, an algorithm based on the GEE coder editor was employed. The code snippets provided in codes 1, 2, and 3 in Appendix 1 detail the process of extracting the concentrations of NO_2, CO, and SO_2, respectively, using the differential optical absorption spectroscopy (DOAS) technique, which is widely used for remote sensing of atmospheric trace gases. code 4, in Appendix 1, outlines the code utilized for extracting the Land Surface Temperature (LST) data specifically for MODIS, using the split-window technique, which uses two thermal bands to estimate LST. The data and methodologies employed in this research include the collection of data and the utilization of tools throughout the study, as presented in Fig. 2. Preprocessing techniques were applied to the TROPOMI data, involving cloud cover removal and the application of quality control filters. Following this, the data were transformed into tropospheric vertical column densities and spatially averaged within predefined areas of interest. The extraction and retrieval of pollutant concentration levels from S5P TROPOMI datasets were facilitated by the cloud computing capabilities offered by the GEE platform.

3. Results and discussion

3.1. Air pollutants from Sentinel-5P TROPOMI data

This section deals with the estimation of atmospheric pollutants using Sentinel-5P data using cloud computing. Indicators of atmospheric pollution can be assessed using the Sentinel-5P TROPOMI data.

3.1.1. Nitrogen dioxide (NO_2)

NO_2 is a toxic air pollutant that causes severe health impacts and premature death, and it is responsible for tens of deaths annually in Cairo, making it a major health risk in urban and industrial areas. This study utilized offline NO_2 data collected from (January to December 2022), and the spatial distribution of NO_2 in Cairo has a significant correlation with the high concentration of buildings in the urban area as shown in Fig. 3.

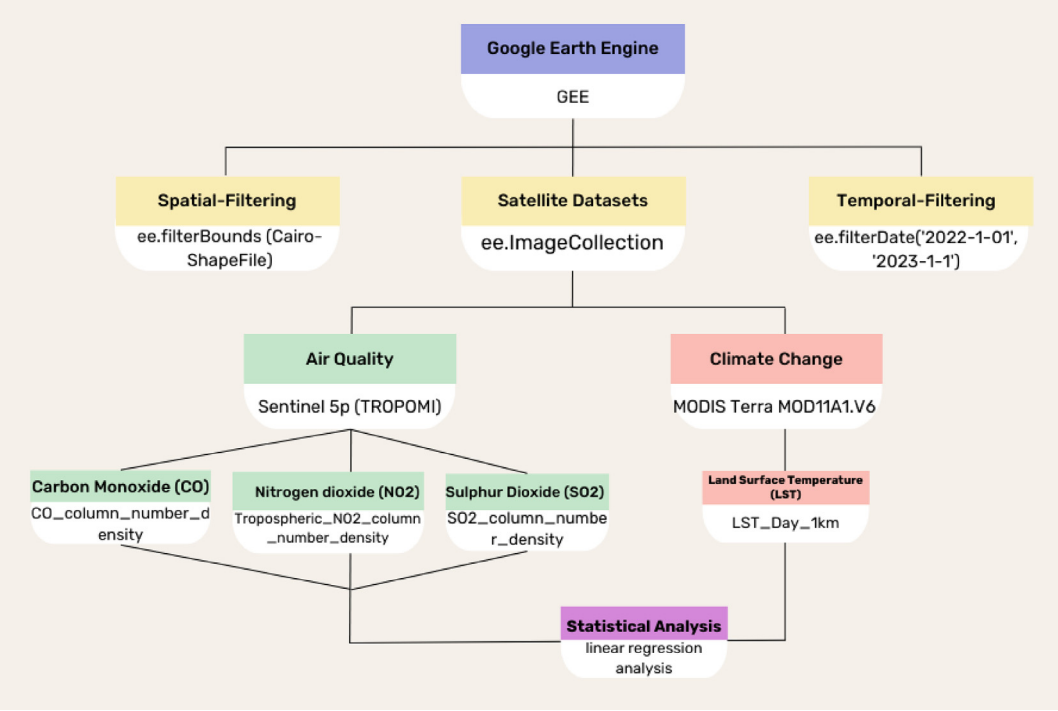

Fig. 2. The data and methodologies flowchart.

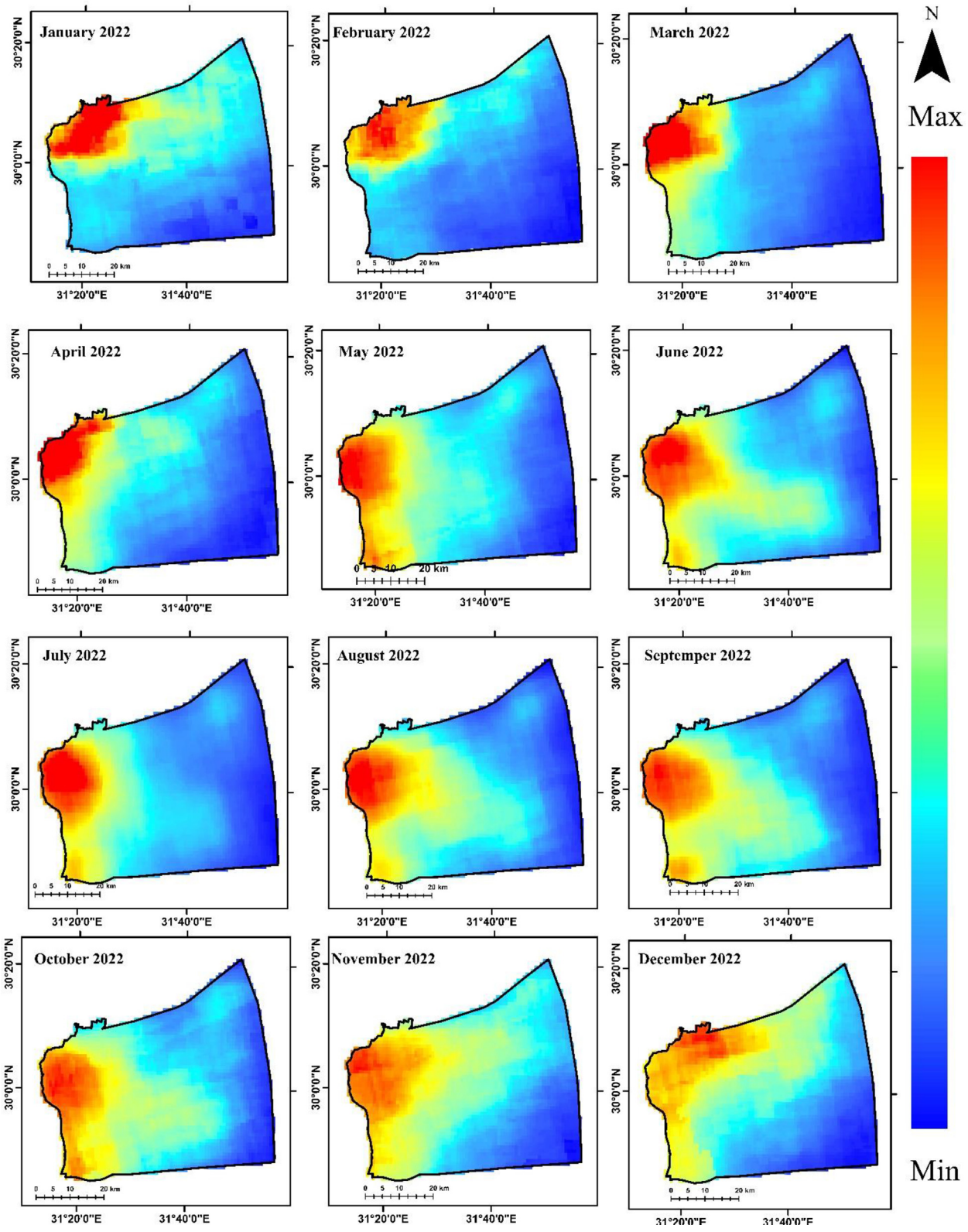

Fig. 3. The monthly distribution of NO_2 concentration in Cairo City for the period January to December 2022.

The NO_2 concentration is primarily concentrated in the east districts, with the highest levels observed near Cairo Airport due to the prevailing northward winds. Notably, the spring season experiences higher wind speeds over the study area. Interestingly, the concentration of NO_2 during spring is typically lower compared with winter. The presence of this pollutant is closely linked to transportation emissions and heating demands this result aligns with the observation of (Hereher et al., 2022), which explains its higher concentrations in densely populated areas with high population density as shown in Fig. 3.

The amount of NO_2 in the atmosphere is linked to several emission sources, such as vehicular emissions and natural sources, and the winter season witnesses the highest concentrations of NO_2 over the study area, where the tropospheric NO_2 gas approaches more than 26*10^4 mol/m^2 in January, and the minimum value of tropospheric NO_2 column density was reported in May, which was 0.41*10^4 mol/m^2, while the concentration in winter is slightly higher than summer months as in Fig. 4.

3.1.2. Carbon monoxide (CO)

The sensitivity of column measurements undergoes variations based on the optical path within cloudy atmospheres, allowing for a convenient estimation using SP5 data sets. In this study, the vertically integrated CO column density at a resolution of 0.01 arc degrees was estimated using Sentinel-5P data. The obtained dataset provided insights into CO concentrations.

The distribution pattern of CO pollutant concentrations, as shown in Fig. 5, is expected to bear similarities to population density and NO_2 pollutant distribution. Notably, CO concentrations predominantly concentrate in the east districts of Cairo, influenced by emissions from motor vehicles and industrial activities. Throughout most of the year, the concentration of this pollutant remains relatively constant at 3.6*10^{-2} mol/m^2, aligning with Mostafa et al.'s (2018) findings, which indicate a peak concentration of CO during the spring season based on monthly averages over 5 years.

These findings suggest a slight increase in CO concentrations during the spring and summer months compared with the winter months. The dataset obtained provided insights into a range of CO concentrations, with the minimum reported value being 0.024 mol/m^2 which was obtained in December and observed peak concentrations of 0.0397 mol/m^2 in March. Analyzing the offline CO data collected from January to December 2022, as depicted in Fig. 6.

3.1.3. Sulfur dioxide (SO_2)

SO_2 gas concentrations in the study area's troposphere, it is primarily associated with industrial and power generation facilities rather than population density and activity. This pattern is particularly noticeable in the northern part of Cairo, where significant textile, smelting, chemical, petroleum industries, and electricity generation plants are located as in Fig. 7. These industrial operations predominantly utilize high sulfur heavy fuel, resulting in the emission of SO_2 and making the region a prominent hotspot for SO_2 emissions (Moseholem, 1992).

The concentration of SO_2 pollutant reaches its highest emission concentration of 0.0088 mol/m^2 in January and December as in Fig. 8. The emissions decreased to the minimum value of 9.61305e-005 in May. While the majority of SO_2 concentration is attributed to emissions from specific industrial activities in North Cairo, surprisingly, some residential areas also experience relatively high levels of

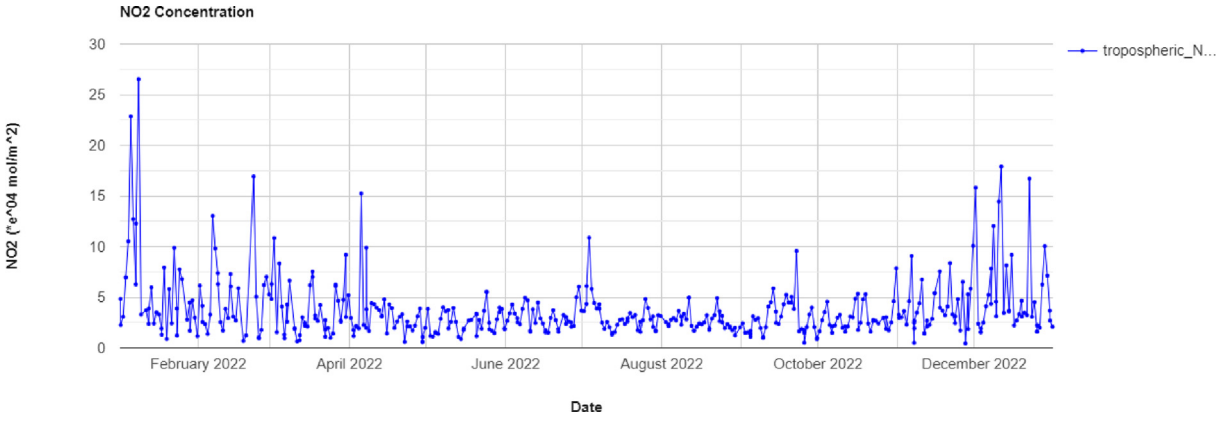

Fig. 4. Diagram of NO_2 concentration from January to December 2022.

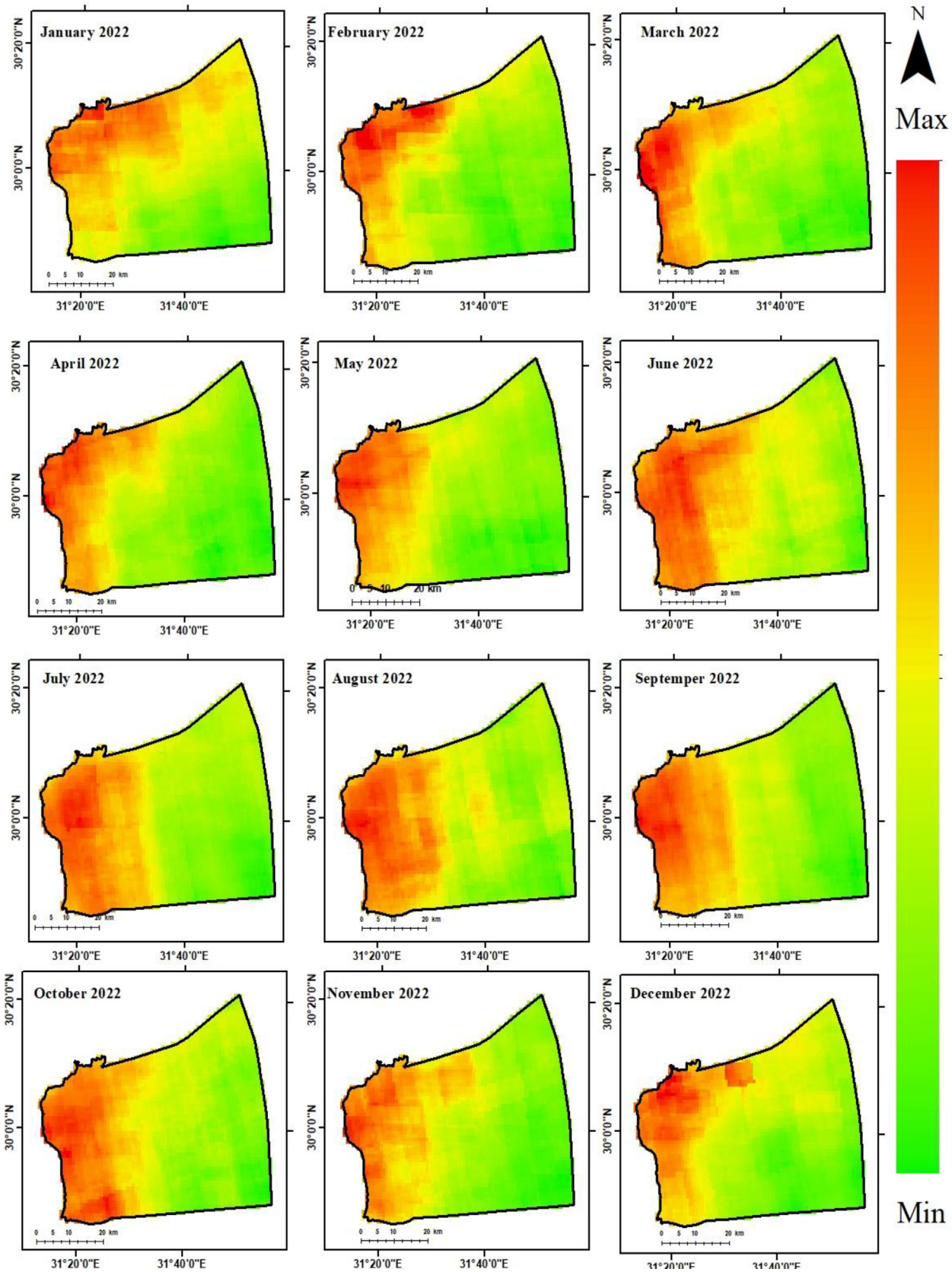

Fig. 5. The monthly distribution of CO concentration in Cairo City for the period January to December 2022.

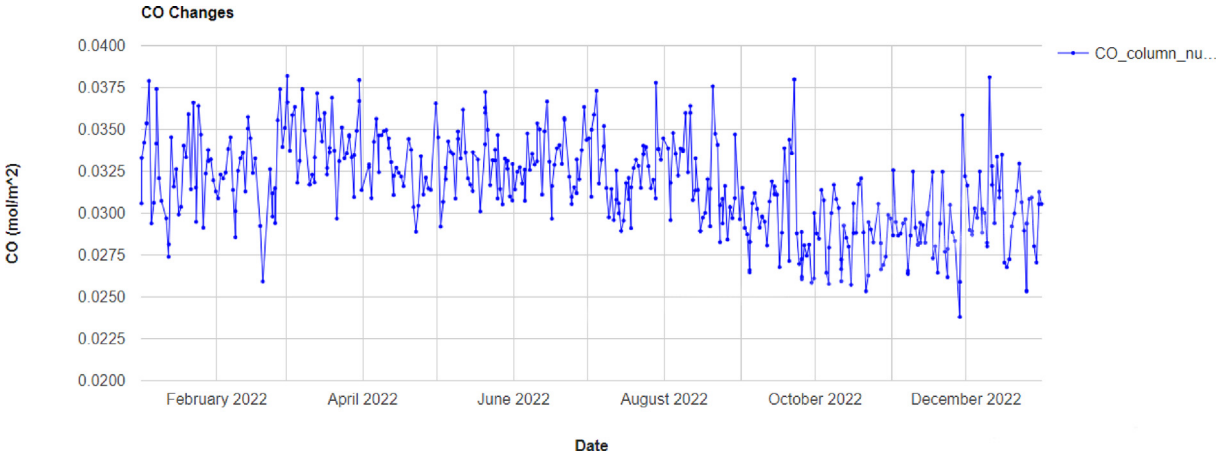

Fig. 6. Diagram of carbon monoxide concentration from January to December 2022.

SO_2. The reason behind these unusually high concentrations of SO_2 in the new urban communities is primarily the extensive use of diesel-fueled trucks for constructing new asphalt roads and carrying out construction activities.

3.2. Land surface temperature from MODIS data

The temperature rise, accompanied by warming and increased LST, can have a profound impact on climate change. Notably, there is an upward trend in temperature, particularly in urban and residential areas, which signifies the influence of human activities on environmental modifications. These findings align with the research conducted by Okeke et al. in 2020 (Okeke et al., 2020). McCarthy et al. (2010) also demonstrated that natural landscapes such as mountains, deserts, and non-urban areas are undergoing a warming process (McCarthy, 2016).

Conversely, a decrease in LST correlates with a reduction in air pollutants, greenhouse gases, and water vapor content. The temporary improvement in air quality, resulting from lower urban temperatures during lockdown measures, establishes a significant connection between human activities, air pollution, particulate matter, radiative flux, and temperature.

The diagram of LST presents that July experienced the highest temperature (60 °C), while November had the lowest temperature (20 °C) in the study area as in (Fig. 9). Based on the study conducted in the area, it was found that the highest levels of air pollution, specifically NO_2, CO, and SO_2, were observed during the colder months of the year similar to the results of (Safarianzengir et al., 2020). This phenomenon can be attributed to temperature inversion. Temperature inversion occurs when a layer of warm air is situated above the colder air near the ground surface. This inversion creates stability in the atmosphere, causing the temperature to increase with altitude instead of the usual decrease. Temperature inversion plays a significant role in air pollution by promoting atmospheric stability, which hinders the vertical movement of pollutants. Additionally, it disrupts the dispersal of pollutants in both vertical and horizontal directions by impeding the movement of air. As a result, when sources of air pollutants, such as vehicles and factories, continuously release their emissions into the lower layer of the atmosphere, the concentration of pollutants sharply rises. The referred situation leads to the highest levels of air pollution occurring when the phenomenon of inversion takes place at low altitudes and persists for extended periods in urban areas. Consequently, this poses a significant threat to human health (Fig. 10).

3.3. Wind influence

The wind direction is a crucial factor influencing air pollution and air quality. The wind speed data for Cairo city is depicted in (Fig. 11). It is observed that the prevailing wind direction in Cairo is from the north. However, it should be noted that wind patterns can exhibit substantial variations among different climate models. While wind direction is an important consideration, it may not be a reliable sole determinant due to the variations (Hulme et al., 2002).

Analyzing Fig. 11, it becomes evident that the wind speed in Cairo plays a significant role in the dispersion of pollution. Considering the industrial nature of the city and the prevailing wind patterns,

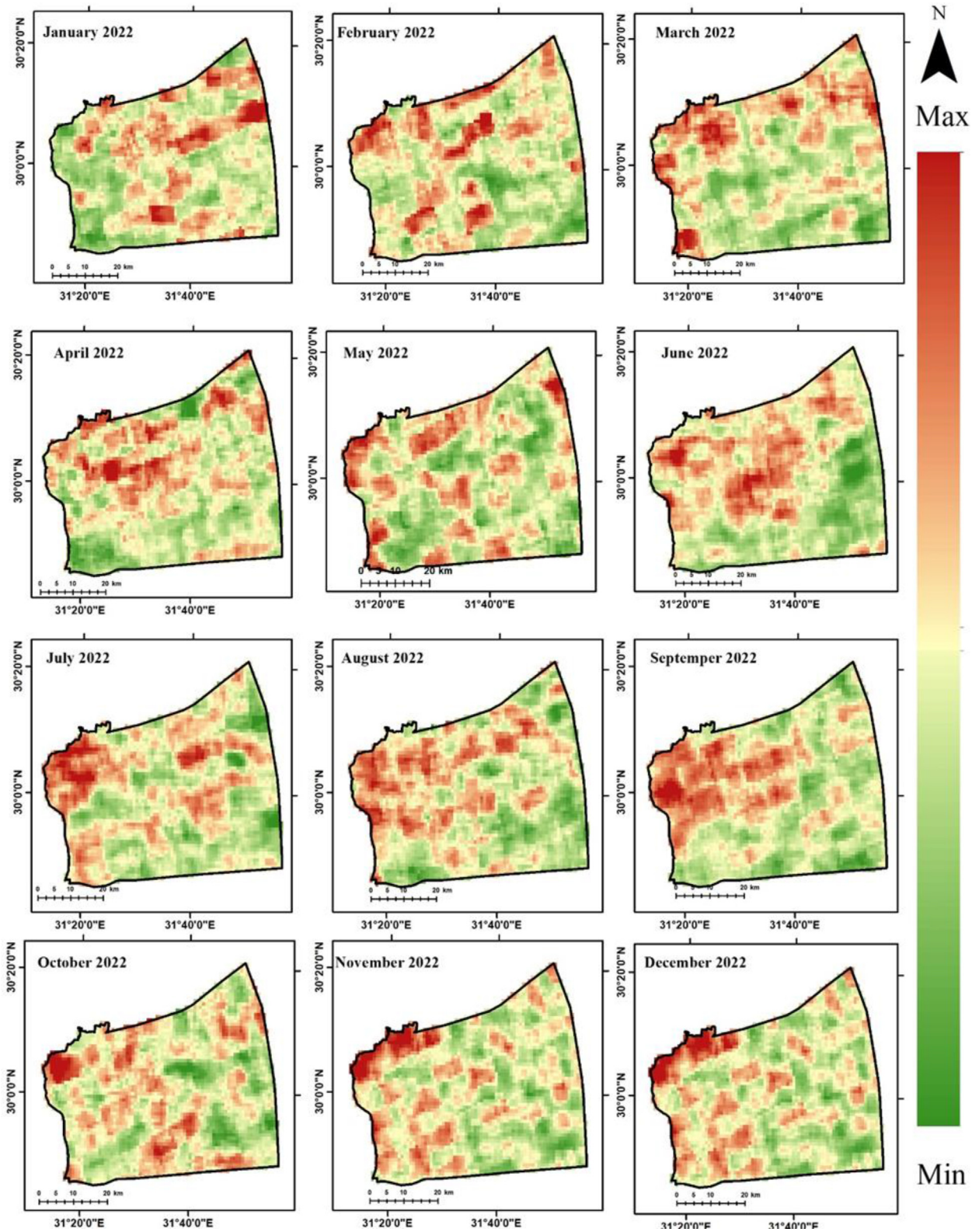

Fig. 7. The monthly distribution of SO_2 concentration in Cairo City for the period January to December 2022.

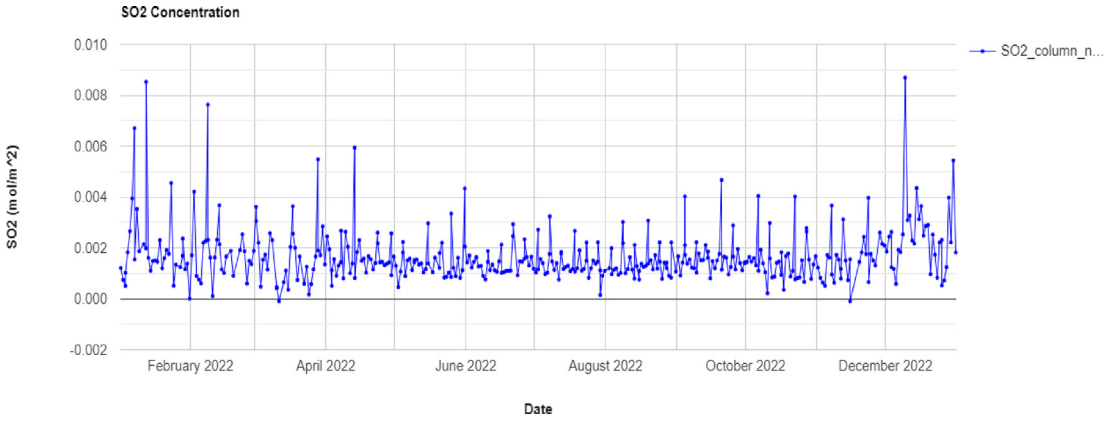

Fig. 8. Diagram of SO_2 concentration from January to December 2022.

it is expected that the spread of pollution in Cairo would be influenced accordingly. The presence of dust on roads is amplified by wind erosion of urban soils that lack adequate protection from surface vegetation and sod layers. As transport speeds on large roads increase and wind intensity grows stronger, fine particles of road dust become suspended in the atmosphere, while the proportion of larger particles gradually rises. Consequently, an expansion in road size and an intensification of traffic flow, particularly on medium to large and major highways, contribute to a reduction in the toxicity equivalence factor (TEF), thereby affecting air quality. This relationship between road characteristics, traffic intensity, and TEF was highlighted (Vlasov et al., 2021).

3.4. Statistical analysis

The Cairo research region was divided into 1512 grids for grid-based regression and scatterplot analysis. Each grid's mean LST, NO_2, CO, and SO_2 concentrations were computed. This approach allowed for a comprehensive examination of the spatial distribution and relationships between these variables across the entire study area. To examine the association between NO_2, CO, SO_2, and LST, Pearson correlation analysis was utilized. Furthermore, linear regression analysis was performed, accompanied by the generation of scatter plots, to enhance our comprehension of the interrelationships among these variables. This approach aimed to provide a more comprehensive understanding of the correlations and patterns between the pollutants and LST.

The scatterplot regression analysis depicted in Fig. 12a–c demonstrates a positive correlation between the mean LST and the mean total concentrations of the studied air pollutants (NO_2, CO, SO_2) in the year 2022. The R-squared values indicate these relationships. Fig. 12a shows a clear positive association between LST and NO_2, with an R-squared value of 0.3757, indicating that NO_2 concentrations are directly influenced by human activities. Similarly, Fig. 12b reveals a positive correlation between CO concentration and mean LST, with an R-squared value of 0.2865. However, the relationship between mean LST and SO_2 Fig. 12c suggests very weak correlation compatibility (Fuladlu and Altan, 2016),

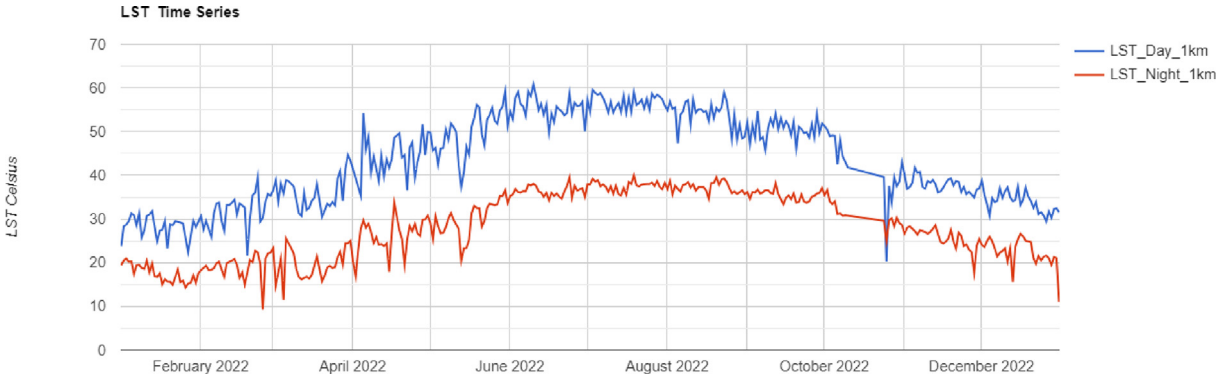

Fig. 9. Diagram of LST changes from January to December 2022.

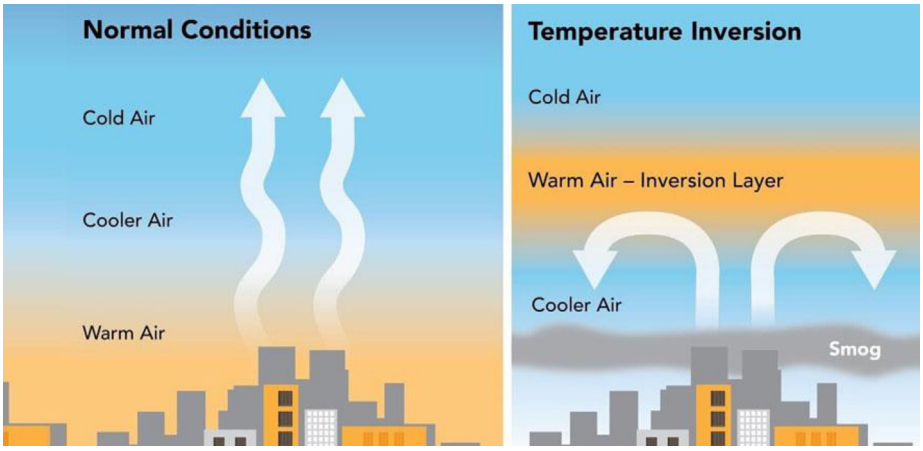

Fig. 10. Temperature inversion phenomenon source: temperature inversion: meaning, definition, causes, effects, and diagram (dashamlav.com).

implying that urban landscape has limited influence on the distribution of this pollutant. The low R-squared value of 0.0129 for SO_2 indicates that the link between LST and SO_2 is negligible. It is important to note that the low R-squared values are due to the regression analysis being based on a single variable, while other environmental factors can affect LST in an urban system. Nonetheless, the findings suggest that greenhouse gases can account for 10 %–30 % of the variation in LST.

3.5. Concentrating air quality forecasting using the exponential smoothing (ETS) algorithm

The collection of real-time air quality data and the availability of air quality forecasts are crucial for implementing preventive and corrective measures, especially in metropolitan cities facing significant air pollution and associated health risks. To address this need, this study proposes a scalable architecture for monitoring and collecting carbon concentration

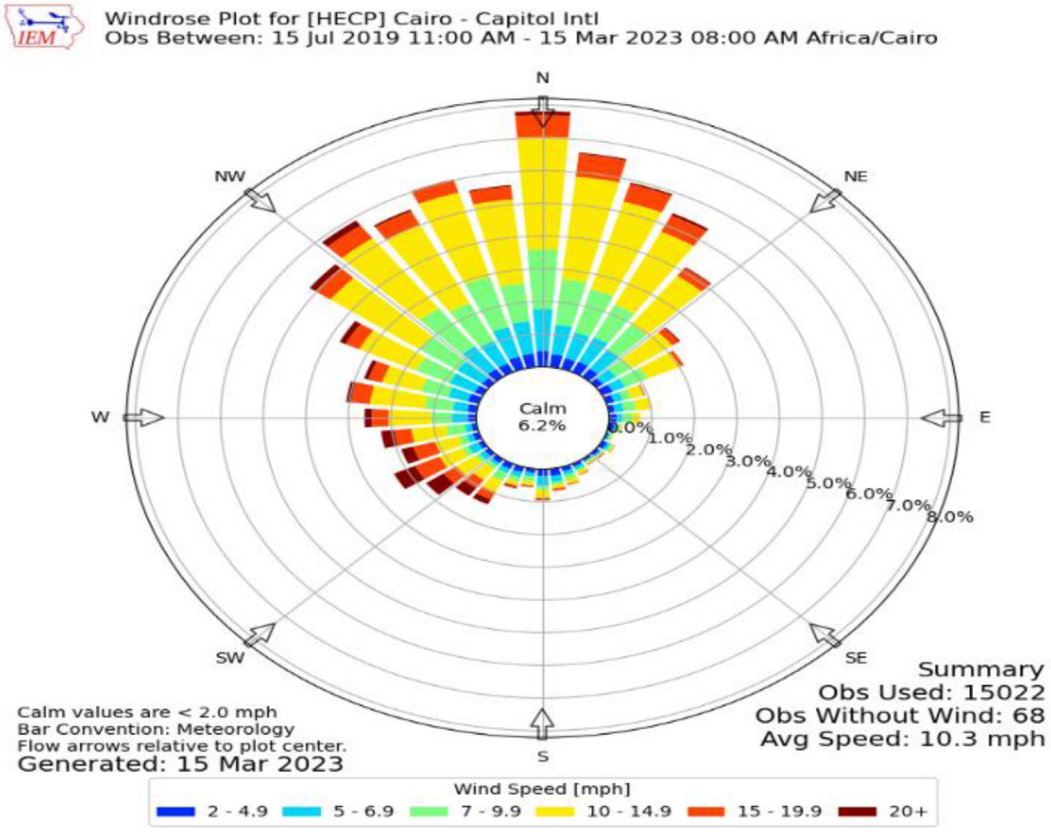

Fig. 11. Wind rose of Cairo City (Source: https://www.mesonet.agron.iastate.edu/sites/windrose.phtml?station=HECP&network=EG__ASOS).

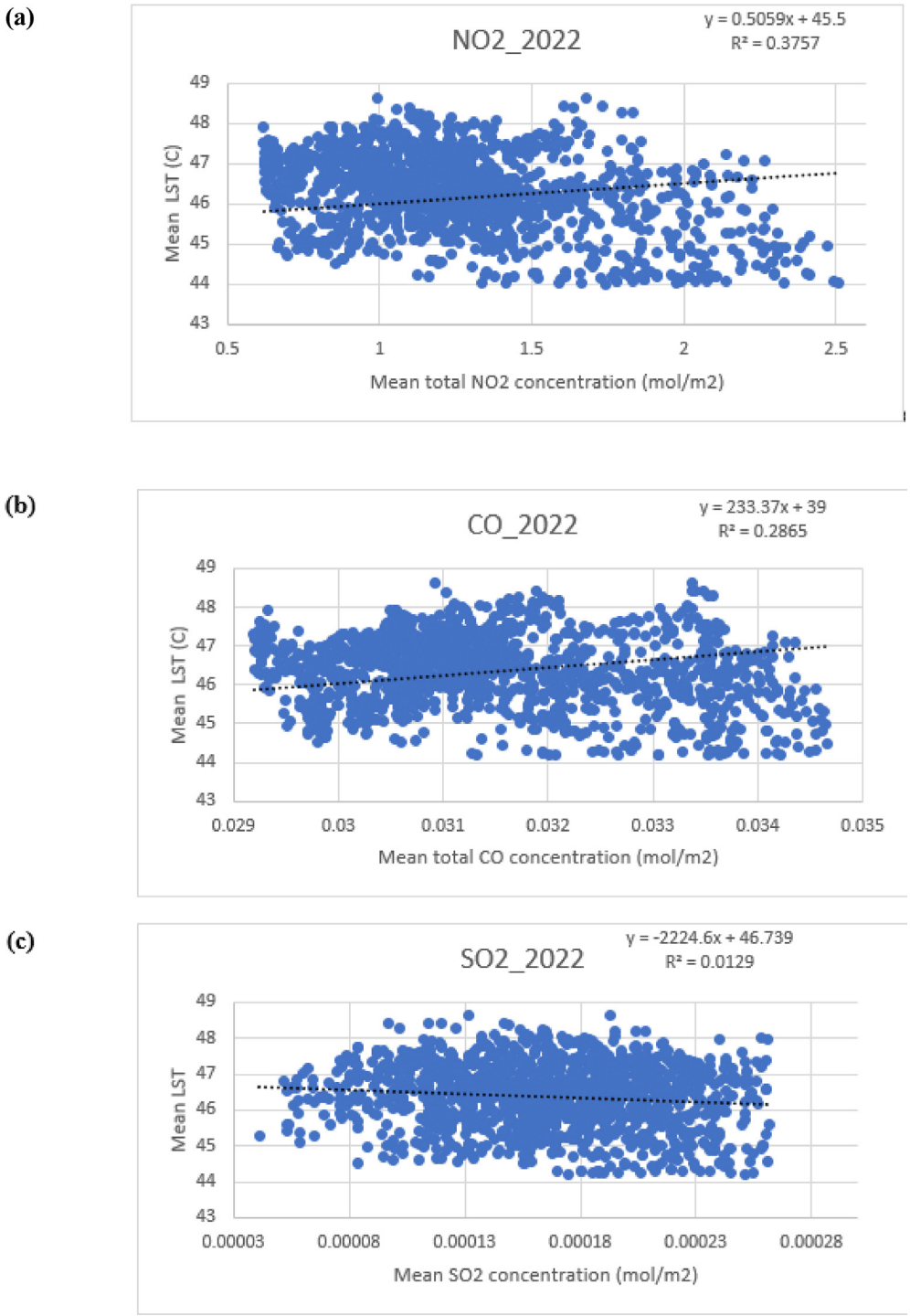

Fig. 12. Grid-based analysis result. The data for the year 2022 has been represented in a scatter plot with the R-squared value. The y axis is the mean LST value and the x axis is (a) Mean NO_2 concentration, (b) Mean CO concentration (c) Mean SO_2 concentration.

data for Cairo. The collected data is then utilized to predict carbon concentrations.

The study utilized real-time air quality data, which was gathered and made accessible, to examine the mean monthly concentrations of various air pollutants. To effectively perform the task of air quality prediction, the ETS algorithm was selected due to its proficiency with time series data. The performance of the models was assessed in the study area, which exhibited noticeable fluctuations

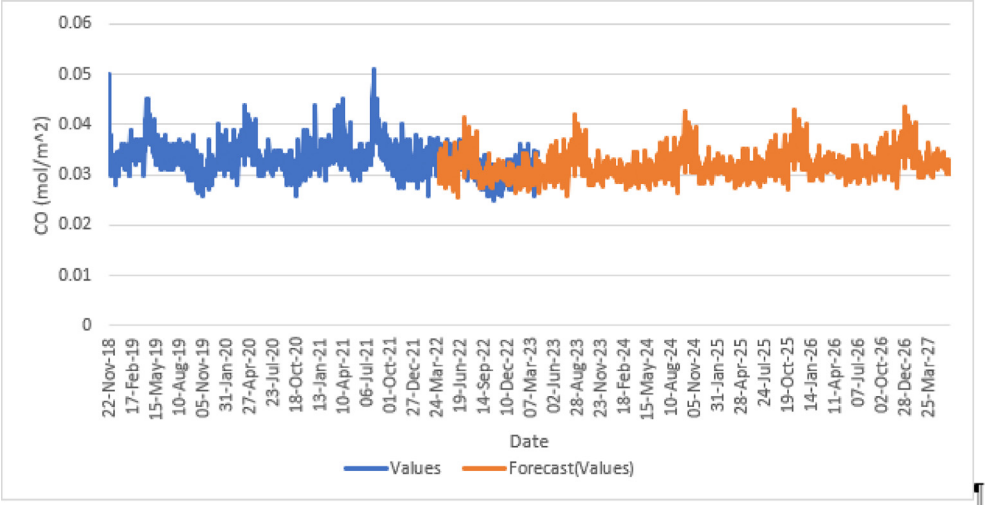

Fig. 13. Testing and predictions using exponential smoothing.

in air quality over time. It was observed that as these oscillations increased, the model's performance suffered, necessitating the use of adaptive modeling techniques.

Based on the observations depicted in Fig. 13, it is evident that the orange line closely aligns with the blue line, indicating a high level of agreement between the predicted values and the actual values. This close alignment signifies a nearly accurate representation, with the predicted values overlapping significantly with the actual values, as visually illustrated in Fig. 13. Additionally, the RMS value for the results is determined to be 0.0036.

Air pollution is a complex problem that requires a multifaceted approach to address. In Cairo, several interventions and policies could be implemented to reduce air pollution levels. One potential intervention is promoting the use of public transportation. Cairo has a high density of cars, which contributes significantly to air pollution levels. Encouraging the use of public transportation, such as buses and trains, could reduce the number of cars on the road and, in turn, reduce air pollution levels. Another potential intervention is implementing stricter regulations on industrial emissions. Industrial activities are a significant source of air pollution in Cairo. By implementing stricter regulations on industrial emissions, the number of pollutants released into the air could be reduced. Encouraging the use of clean energy sources is another potential intervention. The use of fossil fuels is a significant contributor to air pollution in Cairo. By promoting the use of clean energy sources, such as solar and wind power, the number of pollutants released into the air could be reduced. Finally, implementing measures to manage agricultural waste, specifically targeting the control of large-scale rice straw burning, could also help reduce air pollution levels.

3.6. Limitations and future plans

Despite the significant contributions of this study, some limitations need to be addressed in future research. One of the main limitations is the lack of ground-based data, which could have provided more accurate and reliable results. Therefore, future research should focus on collecting more ground-based data to validate the findings of this study. Another limitation is the limited spatial resolution of the Sentinel-5P TROPOMI data, which could have affected the accuracy of the results. Future research should explore the potential of using higher spatial resolution data to improve the accuracy of the results.

In terms of future plans, we aim to expand our study to other cities in Egypt to provide a more comprehensive understanding of air pollution levels in the country. We also plan to explore the potential of using machine learning algorithms to improve the accuracy of our results. Finally, we aim to collaborate with local authorities to develop effective policies and strategies to reduce air pollution levels in Cairo and other cities in Egypt.

3.7. Conclusion

The present study focuses on the spatial and temporal monitoring and analysis of air pollution, specifically pollutants such as NO_2, CO, and SO_2, in the city of Cairo. The eastern research area has the highest NO_2 and CO emissions. Transportation emissions and heating demands in densely populated regions are to responsibility. The northward winds and closeness to Cairo Airport cause these

contaminants to accumulate. Additionally, SO_2 emissions were also higher in the north. Textiles, smelting, chemicals, petroleum, and electricity generation use high-sulfur fuel, which explains this. As a result, this region has become a prominent hotspot for SO_2 emissions. During the 12-month observation period spanning from January to December 2022, the highest levels of NO_2 emissions were recorded in January (26104 mol/m^2), whereas the lowest levels were observed in May (0.41104 mol/m^2). CO emissions peaked in March (0.0397 mol/m^2) and reached their lowest concentration in December (0.024 mol/m^2). As for SO_2, January and December exhibited the highest emissions (0.0088 mol/m^2), while May recorded the lowest value (9.61305e-005). In terms of temperature, July experienced the highest temperature (60 °C), while November had the lowest temperature (20 °C) in the study area. Temperature inversion induced by residential, factory, and home emissions raises pollution levels in winter. However, summer pollutants particularly nitrogen- and sulfur-based vehicle emissions that build closer to the ground pose larger health concerns. In 2022, the mean total NO_2, CO, SO_2, and LST were positively correlated. The mean total NO_2, CO, and SO_2 concentrations had R-squared values of 0.3757, 0.2865, and 0.1774, respectively. These findings indicate that changes in LST explain a significant proportion of the variations observed in the concentrations of these pollutants throughout the year 2022. The Exponential Smoothing (ETS) algorithm showed excellent predictive performance to predict future values of carbon emission till 20 April 2027, with predicted values closely matching actual values. The RMS value for the results was 0.0036, indicating high accuracy. Air pollution in the research location increases childhood respiratory illnesses. Air pollution especially affects children with pre-existing lung problems. Motor vehicle traffic and household heating systems pollute urban air the most. However, careful planning and government assistance can overcome these obstacles.

Author contributions

Conceptualization: M.M. and S.S.; methodology: M.M and S.S and F.Z..; software: S.S.; formal analysis: S.S.; investigation, S.S, AND M.M..; resources, S.S, M.M, AND F.Z..; data curation: S.S.; writing original draft preparation: S.S..; writing review and editing: M.M and F.Z.; statistical Analysis: S.S and F.Z.; supervision: M.M and F.Z.; project administration: M.M. and F.Z.; All authors have read and agreed to the published version of the manuscript.

Funding

This research received no external funding.

Institutional review board statement

Not applicable.

Informed consent statement

Not applicable.

Data availability statement

Code for Air Quality Monitoring: https://code.earthengine.google.com/0d332ed77850449eea417829069724c6.

Code for land surface temperature: https://code.earthengine.google.com/83c3c91b55b258f45f50822c637a189a.

Conflicts of interest

The authors declare no conflict of interest.

Appendix

```
1          //####################  NO2   ###################
2  var collection = ee.ImageCollection('COPERNICUS/S5P/NRTI/L3_NO2')
3    .select('tropospheric_NO2_column_number_density')
4    .filterBounds(geometry)
5    .filterDate('2022-01-01', '2023-01-1')
6     .map(function(img){
7    return img.clip(geometry).multiply(10000).copyProperties(img,
8    ['system:time_start','system:time_end','system:index'])
9  });
10 var averageNO2 = collection.reduce(ee.Reducer.mean())
```

Code 1. NO_2 concentration column density extraction.

```
//###################  CO   ##################
var collection2 = ee.ImageCollection('COPERNICUS/S5P/NRTI/L3_CO')
  .select('CO_column_number_density')
  .filterBounds(geometry)
  .filterDate('2022-01-01', '2023-01-1')
  .map(function(img){
   return img.clip(geometry).copyProperties(img,
   ['system:time_start','system:time_end','system:index'])
});
var averageCO = collection2.reduce(ee.Reducer.mean())
```

Code 2. CO concentration column density extraction.

```
//###################  SO2   ##################
var collection3 = ee.ImageCollection('COPERNICUS/S5P/NRTI/L3_SO2')
  .select('SO2_column_number_density')
  .filterDate('2022-01-01', '2023-01-1')
  .filterBounds(geometry)
  .map(function(img){
   return img.clip(geometry).copyProperties(img,
   ['system:time_start','system:time_end','system:index']);
});
var averageSO2 = collection3.reduce(ee.Reducer.mean())
```

Code 3. SO_2 concentration column density extraction.

```
var modis = ee.ImageCollection("MODIS/061/MOD11A1");

// Define a date range of interest; here, a start date is defined and the end
// date is determined by advancing 1 year from the start date.

var start = ee.Date('2022-01-01');
var end = ee.Date('2023-01-1');
var dateRange = ee.DateRange(start, end);
// Filter the LST collection to include only images intersecting the desired
// date range.
var mod11a2 = modis.filterDate(dateRange);
// Select only the 1km day LST data band.
var modLST = mod11a2.select('LST_Day_1km', 'LST_Night_1km');
print(modLST);
var inCelsius = modLST.map(function(img){
   return img.multiply(0.02).subtract(263.15)
    .copyProperties(img, ['system:time_start']);
});
print('converted', inCelsius);
```

Code 4. LST Extraction From MODIS.

References

Abou-Ali, H., Thomas, A., 2012. Regulating traffic to reduce air pollution in Greater Cairo, Egypt. Econ. Incent. Environ.Regul. 95–119.

Al-alola, S.S., Alkadi II, Alogayell, H.M., Mohamed, S.A., 2022. Environmental and Sustainability Indicators Air quality estimation using remote sensing and GIS-spatial technologies along Al-Shamal train pathway , Al-Qurayyat City in Saudi Arabia. Environ. Sustain Indicat. 15 (January), 100184.

Baldasano, J.M., 2020. COVID-19 lockdown effects on air quality by NO2 in the cities of Barcelona and Madrid (Spain). Sci. Total Environ. 741, 140353.

Bodah, B.W., Neckel, A., Maculan, L.S., Milanes, C.B., Korcelski, C., Ramírez, O., et al., 2022. Sentinel-5P TROPOMI satellite application for NO2 and CO studies aiming at environmental valuation. J. Clean. Prod. 357, 131960.

Borsdorff, T., Aan de Brugh, J., Hu, H., Aben, I., Hasekamp, O., Landgraf, J., 2018. Measuring carbon monoxide with TROPOMI: first results and a comparison with ECMWF-IFS analysis data. Geophys. Res. Lett. 45, 2826–2832.

Burrows, J.P., Weber, M., Buchwitz, M., Rozanov, V., Ladstätter-Weißenmayer, A., Richter, A., et al., 1999. The global ozone monitoring experiment (GOME): mission concept and first scientific results. J. Atmos. Sci. 56, 151–175.

Fuladlu, K., Altan, H., 2016. Examining Land Surface Temperature Relation S to Major Air Pollutant : A R Emote S Ensing R Esearch in C Ase of Tehran.

Garane, K., Koukouli, M.-E., Verhoelst, T., Lerot, C., Heue, K.-P., Fioletov, V., et al., 2019. TROPOMI/S5P total ozone column

data: global ground-based validation and consistency with other satellite missions. Atmos. Meas. Tech. 12, 5263–5287.
Hereher, M., Eissa, R., Alqasemi, A., El Kenawy, A.M., 2022. Assessment of air pollution at Greater Cairo in relation to the spatial variability of surface urban heat island. Environ. Sci. Pollut. Res. 29, 21412–21425. https://doi.org/10.1007/s11356-021-17383-9.
Hulme, M., Adger, W.N., Dessai, S., Goulden, M., Lorenzoni, I., Nelson, D., Wreford, A., 2002. Tyndall centre for climate change research. In: Climate Change Scenarios for the United Kingdom: the UKCIP02 Scientific Report. Tyndall Centre for Climate Change Research, School of Environmental Sciences.
Hwang, J., Maharjan, K., Cho, H., 2023. A review of hydrogen utilization in power generation and transportation sectors: achievements and future challenges. Int. J. Hydrogen Energy 48 (74), 28629–28648.
IPCC, 2021. Contribution of Working Groups I, II and III to the Sixth Assessment Report of the Intergovernmental Panel on Climate Change. https://www.ipcc.ch/report/ar6/wg1/.
Krotkov, N.A., McLinden, C.A., Li, C., Lamsal, L.N., Celarier, E.A., Marchenko, S.V., et al., 2016. Aura OMI observations of regional SO 2 and NO 2 pollution changes from 2005 to 2015. Atmos. Chem. Phys. 16, 4605–4629.
Kurata, M., Takahashi, K., Hibiki, A., 2020. Gender differences in associations of household and ambient air pollution with child health: evidence from household and satellite-based data in Bangladesh. World Dev. 128, 104779.
Leguijt, G., Maasakkers, J.D., Denier van der Gon, H.A.C., Segers, A.J., Borsdorff, T., Aben, I., 2023. Quantification of carbon monoxide emissions from African cities using TROPOMI. Atmos. Chem. Phys. Discuss. 23 (15), 1–27.
Liu, Y., Zhou, Y., Lu, J., 2020. Exploring the relationship between air pollution and meteorological conditions in China under environmental governance. Sci. Rep. 10, 14518.
Liu, Q., Yang, D., Cao, L., 2022. Evolution and prediction of the coupling coordination degree of production–living–ecological space based on land use dynamics in the daqing river basin, China. Sustainability 14, 10864.
Manisalidis, I., Stavropoulou, E., Stavropoulos, A., Bezirtzoglou, E., 2020. Environmental and health impacts of air pollution: a review. Front. Public Health 8. Article 14.
McCarthy, C., 2016. Manage interpretation of medical, forensic evidence in Title IX hearings on campus. Campus Legal Advisor 16, 1–5.
Moseholem, L., 1992. The Arab Republic of Egypt–Environmental Action Plan Preparation Mission: Air Pollution Paper. World Bank, USA.
Mostafa, M.K., Gamal, G., Wafiq, A., 2021. The impact of COVID 19 on air pollution levels and other environmental indicators-A case study of Egypt. J. Environ. Manag. 277, 111496.
Nouri, F., Taheri, M., Ziaddini, M., Najafian, J., Rabiei, K., Pourmoghadas, A., et al., 2023. Effects of sulfur dioxide and particulate matter pollution on hospital admissions for hypertensive cardiovascular disease: a time series analysis. Front. Physiol. 14, 1124967.
Nyaga, E.W., 2021. Aerosol Remote Sensing and Modelling: Estimation of Vehicular Emission Impact on Air Pollution in Nairobi. University of Nairobi, Kenya.
Okeke, F.O., Eziyi, I.O., Udeh, C.A., Ezema, E.C., 2020. City as habitat: assembling the fragile city. Civ. Eng. J 6, 1143–1154.
Rovella, N., Aly, N., Comite, V., Randazzo, L., Fermo, P., Barca, D., et al., 2021. The environmental impact of air pollution on the built heritage of historic Cairo (Egypt). Sci. Total Environ. 764, 142905.
Safarianzengir, V., Sobhani, B., Yazdani, M.H., Kianian, M., 2020. Monitoring, analysis and spatial and temporal zoning of air pollution (carbon monoxide) using Sentinel-5 satellite data for health management in Iran, located in the Middle East. Air Qual. Atmos. Health 13, 709–719.
Sameh, S., Zarzoura, F., El-Mewafi, M., 2023. Automated mapping of urban heat island to predict land surface temperature and land use/cover change using machine learning algorithms: Mansoura city. Int. J. Geoinfo. 18, 6.
Schneising, O., Buchwitz, M., Hachmeister, J., Vanselow, S., Reuter, M., Buschmann, M., et al., 2023. Advances in retrieving XCH 4 and XCO from Sentinel-5 Precursor: improvements in the scientific TROPOMI/WFMD algorithm. Atmos. Meas. Tech. 16, 669–694.
Varma, D.R., Mulay, S., Chemtob, S., 2009. CHAPTER - 20 Carbon monoxide: from public health risk to painless killer. In: Gupta, R.C. (Ed.), Handbook of Toxicology of Chemical Warfare Agents. Academic Press, pp. 271–292.
Veefkind, J.P., Aben, I., McMullan, K., Förster, H., De Vries, J., Otter, G., et al., 2012. TROPOMI on the ESA Sentinel-5 Precursor: a GMES mission for global observations of the atmospheric composition for climate, air quality and ozone layer applications. Remote Sens. Environ. 120, 70–83.
Vlasov, D., Kosheleva, N., Kasimov, N., 2021. Spatial distribution and sources of potentially toxic elements in road dust and its PM10 fraction of Moscow megacity. Sci. Total Environ. 761, 143267.
Vreman, H.J., Wong, R.J., Stevenson, D.K., 2000. Carbon monoxide in breath, blood, and other tissues. Carbon Monoxide Tox. 1, 19–60.
Wen, H., Nie, P., Liu, M., Peng, R., Guo, T., Wang, C., Xie, X., 2023. Multi-health effects of clean residential heating: evidences from rural China's coal-to-gas/electricity project. Energy Sustain. Dev. 73, 66–75.
Xia, C., Liu, C., Cai, Z., Zhao, F., Su, W., Zhang, C., Liu, Y., 2021. First sulfur dioxide observations from the environmental trace gases monitoring instrument (EMI) onboard the GeoFen-5 satellite. Sci. Bull. 66, 969–973.